remote sensing

MDPI

Article

Estimating the Forest Carbon Storage of Chongming Eco-Island, China, Using Multisource Remotely Sensed Data

Chao Zhang [1,2,3,*,†], Tongtong Song [1], Runhe Shi [1,2,3,†], Zhengyang Hou [4], Nan Wu [5], Han Zhang [1] and Wei Zhuo [5]

[1] Key Laboratory of Geographic Information Sciences (Ministry of Education), School of Geographic Sciences, East China Normal University, Shanghai 200241, China; 51203901032@stu.ecnu.edu.cn (T.S.); rhshi@geo.ecnu.edu.cn (R.S.); 51213901012@stu.ecnu.edu.cn (H.Z.)
[2] Key Laboratory of Spatial-Temporal Big Data Analysis and Application of Natural Resources in Megacities, Ministry of Natural Resources, Shanghai 200241, China
[3] Joint Laboratory for Environmental Remote Sensing and Data Assimilation, East China Normal University, Shanghai 200241, China
[4] The Key Laboratory for Silviculture and Conservation (Ministry of Education), Beijing Forestry University, Beijing 100083, China; houzhengyang@bjfu.edu.cn
[5] School of Geography and Tourism, Anhui Normal University, Wuhu 241000, China; wunan@ahnu.edu.cn (N.W.); weizhuo1121@ahnu.edu.cn (W.Z.)
* Correspondence: zhangchao@geo.ecnu.edu.cn; Tel.: +86-21-5434-1218
† These authors contributed equally to this work and should be considered co-first authors.

Abstract: Urban forests are highly heterogeneous; information about the combined effect of forest classification scale and algorithm selection on the estimation accuracy for urban forests remains unclear. In this study, we chose Chongming eco-island in the mega-city of Shanghai, a national experimental carbon neutral construction plot in China, as the study object. Remote sensing estimation models (simple regression models vs. machine learning models) of forest carbon density were constructed across different classification scales (all forests, different forest types, and dominant tree species) based on high-resolution aerial photographs and Sentinel-2A remote sensing images, and a large number of field surveys and optimal models were screened by ten-fold cross-validation. The results showed that (1) in early 2020, the total forest area and carbon storage of Chongming eco-island were 307.8 km^2 and 573,123.6 t, respectively, among which the areal ratios and total carbon storage ratios of evergreen broad-leaved forest, deciduous broad-leaved forest, and warm coniferous forest were 51.4% and 53.3%, 33.5% and 32.8%, and 15.1% and 13.9%, respectively. (2) The average forest carbon density of Chongming eco-island was 18.6 t/ha, among which no differences were detected among the three forest types (i.e., 17.2–19.2 t/ha), opposite to what was observed among the dominant tree species (i.e., 14.6–23.7 t/ha). (3) Compared to simple regression models, machine learning models showed an improvement in accuracy performance across all three classification scales, with average rRMSE and rBias values decreasing by 29.4% and 53.1%, respectively; compared to the all-forests classification scale, the average rRMSE and rBias across the algorithms decreased by 25.0% and 45.2% at the forest-type classification scale and by 28.6% and 44.3% at the tree species classification scale, respectively. We concluded that refining the forest classification, combined with advanced prediction procedures, could improve the accuracy of carbon storage estimates for urban forests.

Keywords: eco-island; carbon storage; carbon density; Sentinel-2A; spatial pattern

Citation: Zhang, C.; Song, T.; Shi, R.; Hou, Z.; Wu, N.; Zhang, H.; Zhuo, W. Estimating the Forest Carbon Storage of Chongming Eco-Island, China, Using Multisource Remotely Sensed Data. *Remote Sens.* **2023**, *15*, 1575. https://doi.org/10.3390/rs15061575

Academic Editors: Nancai Pei, Qian (Chayn) Sun, Jiali Jin and Zezhou Hao

Received: 20 January 2023
Revised: 1 March 2023
Accepted: 9 March 2023
Published: 14 March 2023

1. Introduction

Cities account for less than 1% of the Earth's surface but produce more than 70% of global carbon dioxide (CO_2) emissions [1]. Urban forests, consisting of forest patches, forest strips, and scattered trees, are natural and artificial ecosystems within cities and form an important component of urban green infrastructure [2]. Through photosynthesis, urban forests

absorb CO_2 which is then stored within plants and this means of carbon sequestration represents an important nature-based solution in adapting to climate change [3,4].

Numerous studies have demonstrated the effectiveness of remote sensing, including optical, LiDAR, and microwave-based approaches, in estimating urban forest carbon storage [5–8]. However, optical remote sensing is currently the most commonly used method in estimating carbon storage in urban areas due to the wide variety of available data, accessibility, and intuitive presentation [9]. Estimation of the accuracy of this approach has been a frequent focus due to the highly heterogeneous characteristics of urban forests [10,11]. Landsat imagery has frequently been used with various regression algorithms [12–14] and high-spatial-resolution images (e.g., Sentinel-2) combined with advanced algorithms (e.g., machine learning algorithms) have been widely applied in recent years [15–17], whereas, to date, whether different forest classification scales (all forests, forest types, and tree species) affect the estimation accuracy, especially in different algorithms, has received limited attention [18].

China, together with other developing countries, is now leading the current global carbon emission trend and aims to reach carbon neutrality by 2060. Shanghai, one of China's mega-cities, is leading with regard to the carbon peaking and neutrality goals in China, and one main work has been to initiate the estimation and management of natural carbon storage [19], whereas previous studies have mainly focused on coastal wetland vegetation estimations based on field ground surveys and/or remote sensing methods [20,21]. A few forest carbon storage estimation studies in Shanghai have been conducted based on field investigation data [22,23]. In the past three years, remote sensing methods have been used to estimate forest carbon storage in Shanghai [11,24]; however, such studies have all been based on Landsat images and limited field ground samples (e.g., a total of 92 field samples for Shanghai). Given the high heterogeneity of urban forests, the accuracy of the current estimation needs to be improved [25].

Chongming eco-island, within the administrative title of Chongming District, is the largest district of Shanghai (i.e., 22.3% of the total area of Shanghai). The initiation of this eco-island construction started in 2005, and this target was raised to be a world-class eco-island in 2018; a pioneer area of low carbon development nationally [26,27], this eco-island is of global significance and gained global repute [28]. The forest area accounted for approximately 27% of the terrestrial area of this eco-island in 2019. In the context of the national carbon peaking and carbon neutrality goals, the local government recently committed to taking the leading role in building this eco-island to be a carbon-neutral demonstration zone; consequently, the following questions were asked: (1) How much forest carbon is currently stored in this eco-island? (2) Can the accuracy of the estimation be affected by the choice of forest classification scales and different algorithms?

In this study, we aimed to identify the combined effect of forest classification scale and algorithm selection on the estimation accuracy of urban forests. For this purpose, we chose Chongming eco-island as the study object, and remote sensing estimation models (simple regression models vs. machine learning models) of forest carbon density were constructed across different classification scales (all forests, different forest types, and dominant tree species) based on high-resolution aerial photographs, Sentinel-2A remote sensing images, and a large number of field surveys. The spatial distribution characteristics of forest carbon density were analyzed, the estimation accuracies among different models and across different forest classification schemes were compared, and carbon improvement targeted forest management measures were subsequently proposed.

2. Materials and Methods

2.1. Study Area

Chongming eco-island (121°09′30″–121°54′00″N, 31°27′00″E–31°51′15″E) is located in Northern Shanghai, surrounded by the northern and southern branches of the Yangtze River and the East China Sea (Figure 1). This eco-island consists of Chongming Island (the

world's largest estuarine alluvial island), Changxing Island, and Hengsha Island and has a flat and homogeneous terrain in the elevation range of 3.5–4.5 m [29].

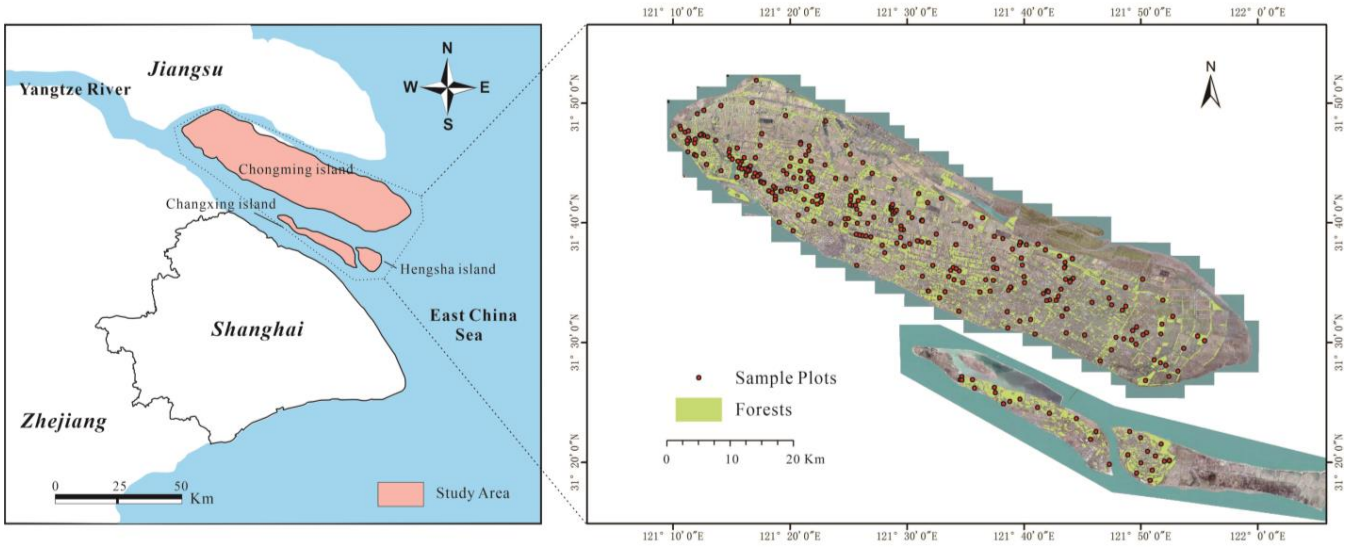

Figure 1. Geographical location of Chongming eco-island and the spatial distribution of forests (green part) and field sample plots (red dots) on the eco-island.

The climate is a subtropical monsoon climate, and the mean annual temperature is 16.5 °C; the highest temperature occurs in July with an average value of 26.9 °C, and the lowest temperature occurs in January with an average value of 3.5 °C. The average annual rainfall is 1128.9 mm, mainly distributed between April and September [30]. The zonal vegetation consists of subtropical evergreen–deciduous broad-leaved mixed forests [31], and currently, the local forest vegetation is mainly artificially planted [29]. Wildfires and deforestation are not present on this eco-island.

2.2. Remote Sensing Images

Sentinel-2 is a high-resolution, multi-spectral imaging mission with a wide swath of coverage that is operated by the European Space Agency. The mission's spectral imager spans 13 spectral bands. In this study, Sentinel-2A data (https://scihub.copernicus.eu/dhus/#/home, accessed on 3 May 2020) were selected as remote sensing images. First, images covering Chongming eco-island across the forest growth period (April–October) from 2020 to 2021 were downloaded, and three date images (two images each date) (Table S1) were finally selected based on the standard of cloud coverage being less than 4%. Second, the correlation between the carbon density of the ground-measured sample and each vegetation index of the corresponding coordinates of these three date images was calculated, and the date images taken on 3 May 2020 with the highest correlation (the track numbers of which are R089 and the stitching domain numbers are T51SUR and T51RUQ) were chosen as the base images. The official L1C-level data, which have been orthorectified and geometrically corrected, were (the 10 m and 20 m resolution bands were used in this study) atmospherically corrected using the Sen2cor plug-in released by ESA and then resampled to 10 m using the image processing package SNAP developed by ESA for processing Sentinel data.

2.3. Forest Classification and Mapping

In this study, forest mapping (different forest types and dominant tree species) was conducted using a combination of manual visual interpretations and field surveys based on aerial photographs obtained from the Shanghai Surveying and Mapping Institute. The photographs were taken using a Digital Mapping Camera III (Z/I Imaging, Huntsville, AL, USA) with RGB and 1 m resolution, resulting in a total of 424 images captured

between November 2019 and February 2020 [32]. Based on the literature regarding forest vegetation in Chongming [33,34], "Vegetation of China" (China Vegetation Editorial Committee, 1980) [31] and our extensive field survey, the forest vegetation was divided into three types: evergreen broad-leaved forest (hereafter EBLF), deciduous broad-leaved forest (hereafter DBLF), and warm coniferous forest (hereafter WCF). Additionally, five dominant tree species (*Cinnamomum camphora*, *Ligustrum lucidum*, *Sapindus Saponaria*, *Metasequoia glyptostroboide*, and *Taxodium distichum var. imbricatum*), the distribution ratios of which exceeded 5% of the total forest area, were also extracted and mapped.

2.4. Model Independent Variables

Compared to ordinary optical satellites, Sentinel-2A contains three red-edge bands [35]; therefore, in this experiment, we deliberately added 5 red-edge vegetation indices in addition to the common conventional vegetation indices. Based on a literature survey [35–37], a total of 19 spectral indices (4 spectral reflectivity and 15 vegetation indices, Table S2) with significant correlations to forest carbon density were selected in this study as candidates for estimating carbon storage.

2.5. Field Survey and Ground Carbon Density Estimation

After the forest mapping work finished at the end of 2020, a highly intensive field survey of plant communities was conducted from March to August 2021 (Figure S1), and a total of 308 sample plot (20 × 20 m) surveys were performed. The survey steps mainly followed the method described by Chen et al. (2018) [38]: (1) points were randomly created on the forest distribution map (aerial photograph) using ArcGIS, and the location of each point (coordinate) was subsequently treated as the center of each community sample plot; (2) the location of each point (i.e., the coordinates) was found based on the geographical distribution traits (e.g., roads, rivers, and buildings) and coordinate positioning (RTK-Trimble R2, USA), and each sample plot (20 × 20 m) was set; and (3) the plant community structural parameters (i.e., the tree species name, tree height, and stem diameter (at stem height 1.3 m from the ground)) were investigated for each individual tree in each plot.

The forest carbon storage in each plot (CS_{plot}) was obtained as the sum of the carbon storage of every tree, which was obtained by multiplying the tree biomass and the carbon content coefficient (Equation (1); Table S3), and the carbon density of each plot or island was obtained by dividing the total carbon storage (of the plot or island) by its corresponding area. The aboveground biomass of every tree was calculated by the allometric biomass equations of each tree species (using its height and/or diameter as independent variables, Table S4), and if a species-specific equation was not available, we selected a possible equation from a tree species belonging to the same genus or family [39]. Basic information regarding the carbon densities for the 308 plots is shown in Table 1.

$$CS_{plot} = \sum_{j} \sum_{i} B_{ij} \times C_i \quad (1)$$

where B_{ij} represents the biomass of the jth plant of the ith tree species in each plot and C_i represents the carbon content coefficient of the ith species in the corresponding sample plot.

Table 1. Summary of the variability of the carbon densities (t/ha) of the 308 plots.

Classification Scale		Number of Plots	Minimum Value (t/ha)	Maximum Value (t/ha)	Mean Value (t/ha)	SD (t/ha)
Dominant tree species	*Cinnamomum camphora*	69	8.8	67.4	26.2	14.8
	Ligustrum lucidum	25	7.5	20.1	13.3	4.7
	Sapindus saponaria	23	8.5	52.8	23.3	12.5
	Metasequoia glyptostroboides	32	11.8	68.0	21.7	17.8
	Taxodium distichum var. imbricatum	21	4.7	46.2	17.1	15.0

Table 1. *Cont.*

Classification Scale		Number of Plots	Minimum Value (t/ha)	Maximum Value (t/ha)	Mean Value (t/ha)	SD (t/ha)
Forest type	Evergreen broad-leaved forest	130	5.4	67.4	21.5	15.2
	Deciduous broad-leaved forest	106	3.9	63.2	19.4	16.9
	Warm coniferous forest	72	3.5	68.0	18.3	17.4
All forests		308	3.5	68.0	19.9	16.3

2.6. Model Construction

To avoid the influence of other land use types, we established a forest mask in the images of each remote sensing feature variable. The forest distribution on Chongming eco-island was relatively scattered, and forest patches were generally homogeneous as a result of human plantation activities, a fixed carbon density value was assigned to each plot (20 × 20 m), and this value was used to fit four pixels (10 × 10 m) in the analysis. The correlation direction and degree between each candidate variable and forest carbon density at different classification scales (i.e., all forests, different forest types, and dominant tree species) were examined by Pearson correlation analysis before constructing the model (Table S5), and the feature variables with the highest correlation coefficients were ranked according to the absolute value of the correlation coefficients.

To address the challenge of the high heterogeneity of urban forests, we chose three common simple regression models (the simple regression model (SR), multiple linear stepwise regression model (MSR), and exponential regression model (ER)) and three mainstream machine learning models (the random forest model (RF), decision tree model (DT), and neural network model (NN)) to estimate the carbon density of each pixel at three different classification scales. The correlations between the spectral indices and carbon density were analyzed first. The spectral indices with the highest correlation coefficients then participated in the SR and ER construction, and spectral indices with strong correlations ($R > 0.5$) (passing the multicollinearity test) participated in the MSR and machine learning model construction. The inversion models used to estimate carbon density at three different classification scales were further identified based on the equation with the highest accuracy among the analyzed equations.

To evaluate the accuracy of each model, we used a random sampling method in which the 308 ground truth samples were divided into a training set and a test set at a ratio of 7:3. Then, each model was trained and optimized using 10-fold cross-validation. The root mean square error (RMSE), relative root mean square error (rRMSE), bias (Bias), relative bias (rBias), and the coefficient of determination (R^2) were calculated in MATLAB 2019a (TreeBagger package for RF, fitrtree package for DT, and feedforwardnet package for NN) to compare the prediction performances of the different models at different forest scales. In turn, according to the results, the models with the highest accuracies (lowest rRMSE and rBias and highest R^2) (Equations (2)–(6)) were fitted at different taxonomic scales to obtain a carbon density distribution map:

$$\mathrm{RMSE} = \sqrt{\frac{\sum_{i=1}^{n}(\hat{y}_i - y_i)^2}{n}} \tag{2}$$

$$\mathrm{rRMSE} = \frac{\mathrm{RMSE}}{\overline{y}} \cdot 100 \tag{3}$$

$$\mathrm{Bias} = \frac{\sum_{i=1}^{n}(\hat{y}_i - y_i)}{n} \tag{4}$$

$$\mathrm{rBias} = \frac{\mathrm{Bias}}{\overline{y}} \cdot 100 \tag{5}$$

$$R^2 = 1 - \frac{\sum_{i=1}^{n}(y_i - \hat{y}_i)^2}{\sum_{i=1}^{n}(y_i - \overline{y})^2} \quad (6)$$

where y_i is the ith observed carbon density value, $\hat{y}_i$ is the ith estimated carbon density value, $\overline{y}$ is the mean of all the observed carbon density values, and n is the number of observations. Generally, lower RMSE and Bias values and higher R^2 values indicate a better estimation accuracy.

3. Results

3.1. Distribution of Forest Types and Dominant Tree Species

The total forest area of Chongming eco-island was 307.80 km^2, approximately 27% of the total terrestrial area. More specifically, the areas (coverage ratios) of Chongming Island, Changxing Island, and Hengsha Island were 259.7 km^2 (25%), 27.3 km^2 (33%), and 20.8 km^2 (41%), respectively (Figure 2a). Regarding Chongming Island, the forest coverage ratios were higher in the western and southern regions than in the eastern and northern regions, and one distinctive trait was its distribution along coastal dams around the island, traffic roads (e.g., Chenhai highway and Beiyan highway), and river channels (e.g., the South Hengyin River and the North Hengyin River). The forests distributed on Changxing Island were concentrated in its western region. The forests on Hengsha Island were distributed mainly along the coastal roads around the island.

The areas of evergreen broad-leaved forest (EBLF), deciduous broad-leaved forest (DBLF), and warm coniferous forest (WCF) were 158.2 km^2, 103.1 km^2, and 46.5 km^2, respectively. Large EBLF areas could be observed on the three islands, WCF was distributed mainly on Chongming Island with a band-like distribution, and DBLF was also distributed mainly on Chongming Island in small patches (Figure 2a).

The total area of five major tree species (*C. camphora*, *L. lucidum*, *S. saponaria*, *M. glyptostroboides*, and *T. distichum var. imbricatum*) was 189.2 km^2, accounting for 61.4% of the total forest area (Figure 2b), and *C. camphora* had the largest area (approximately 30% of total forest area) with a relatively even distribution among the three islands, especially on Chongming Island. *M. glyptostroboides* and *T. distichum var. imbricatum* were distributed mainly along coastal dams around the islands and along traffic roads and river channels with a band-like distribution. *L. lucidum* and *S. saponaria* were distributed mainly in the central and western regions of Chongming Island in small patches, and a few distribution areas could be observed on Changxing Island and Hengsha Island.

3.2. Correlation of Candidate Variables with Forest Carbon Density

The correlation coefficients between each variable and the corresponding carbon density of each sample plot in the three contexts are shown in Table S5. The correlation coefficients between spectral variables and carbon density at refined classification scale (i.e., forest type and tree species) were significantly higher than those at the all-forest scale, the average correlation coefficient in warm coniferous forests was the highest (R = 0.529), and the average correlation coefficient in all forest was the lowest (R = 0.467). Among the three forest types, ARVI and reNDVI had the highest correlation coefficients (with a mean correlation coefficient higher than 0.6). Predictive variables identified for carbon density estimation for three simple regression models and machine learning models are presented in Tables S6 and S7, respectively.

3.3. Carbon Density Estimation Models

3.3.1. Simple Regression Models

The RMSE, rRMSE, Bias, and rBias values derived at different classification scales are shown in Table 2. The rRMSE values of each simple regression model were larger than 30% except for those obtained for *C. camphora*, and all of the rBias values were in the range of 0.6–2.8%. The prediction accuracy was low. The prediction accuracy values at the forest type and tree species scales were generally higher than those at the all-forest scale;

more specifically, the rRMSE and rBias values of the three simple prediction models at the all-forest scale were 48.33% and 2.35%, respectively. Compared to the all-forest scale, at the forest type scale, the rRMSE and rBias values decreased by 22.47% and 36.73%, respectively, and R^2 increased by 19.59%; at the dominant tree species scale, the rRMSE and rBias values decreased by 25.59% and 34.82%, respectively, and R^2 increased by 15.67%.

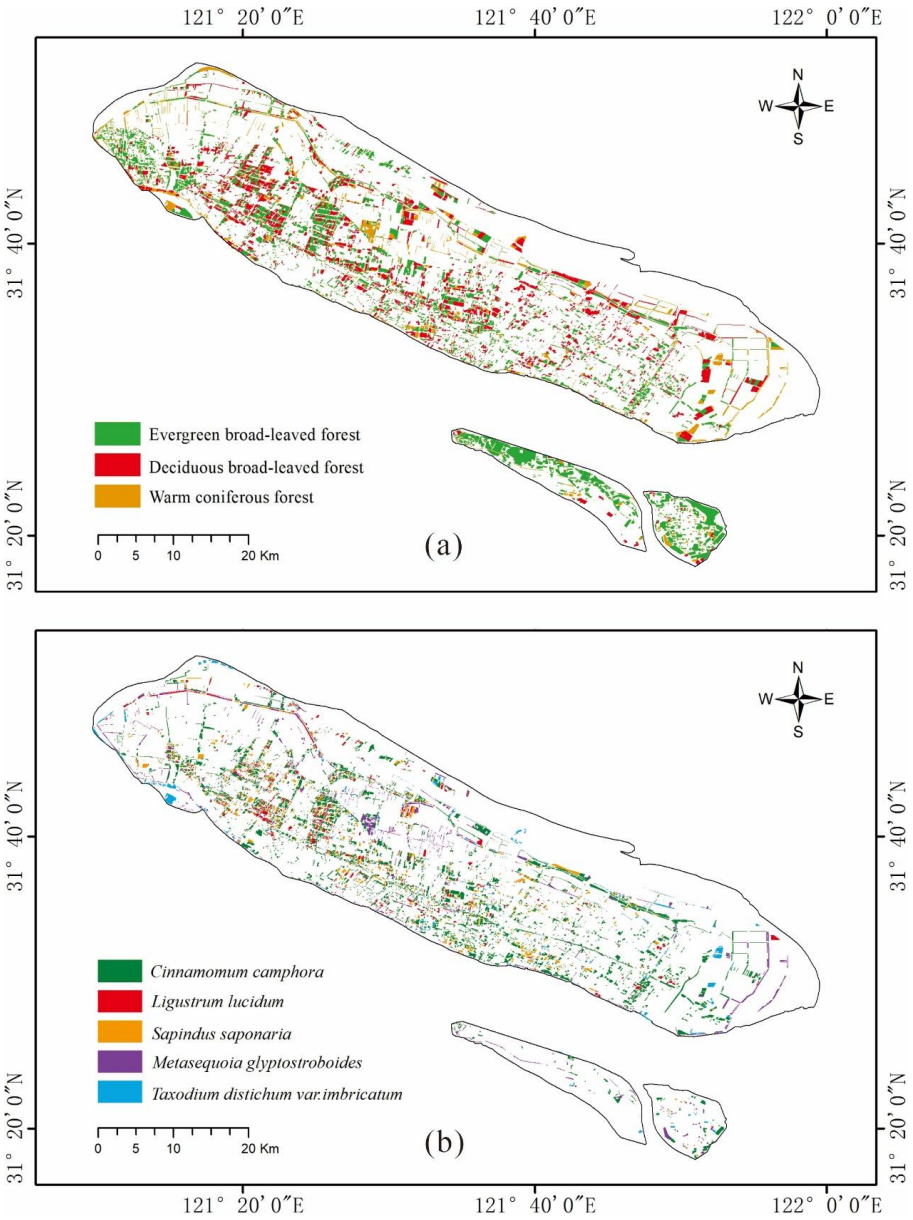

Figure 2. Spatial distributions of (**a**) three forest types and (**b**) dominant tree species on Chongming eco-island.

3.3.2. Machine Learning Models

The average RMSE, rRMSE, Bias, and rBias values of the three machine learning models at different classification scales are shown in Table 3. Except for the all-forest classification scale, the rRMSE value of each machine learning model was less than 40%, and the rBias value was less than 1.8%; these prediction accuracies were thus significantly improved compared to those derived from the simple regression models (Table 2). Additionally, the prediction accuracy values at the forest type and tree species scales were generally higher than those values at the all-forest scale; more specifically, the rRMSE and rBias values of the three machine learning models at the all-forest scale were 36.87% and 1.58%, respectively.

Compared to the results obtained at the all-forest scale, at the forest type scale, the rRMSE and rBias values decreased by 28.37% and 58.23%, respectively, and R^2 increased by 22.60%; at the dominant tree species scale, the rRMSE and rBias values decreased by 32.62% and 58.54%, respectively, and R^2 increased by 21.07%. Among these three models, RF was the optimal model for all forests, EBLF, WCF, and *C. camphora*; DT performed best for DBLF and the other four dominant tree species.

Table 2. Comparison of accuracy values of carbon density among different models and across different forest classification schemes. EBLF: evergreen broad-leaved forest, DBLF: deciduous broad-leaved forest, WCF: warm coniferous forest, SR: simple regression model, ER: exponential regression model, MSR: multiple linear stepwise regression model.

Classification Scale		Model Name	RMSE (t/ha)	rRMSE (%)	Bias (t/ha)	rBias (%)	R^2
Forest type	All forests	SR	12.71	51.44	0.69	2.74	0.24
		ER	11.52	46.08	−0.56	−2.23	0.35
		MSR	12.37	47.48	0.53	2.11	0.38
	EBLF	SR	10.91	42.12	0.47	1.82	0.23
		ER	8.43	32.55	0.53	2.03	0.44
		MSR	9.62	36.86	−0.32	−1.22	0.53
	DBLF	SR	11.45	40.03	−0.54	−1.89	0.31
		ER	9.09	31.78	0.28	0.99	0.42
		MSR	12.35	41.99	−0.33	−1.16	0.29
	WCF	SR	11.49	43.20	0.52	1.94	0.33
		ER	8.35	31.23	0.34	1.28	0.47
		MSR	9.97	37.48	−0.30	−1.11	0.46
Dominant tree species	*Cinnamomum camphora*	SR	10.93	30.07	0.41	1.10	0.39
		ER	9.21	24.53	0.22	0.64	0.47
		MSR	9.93	26.4	−0.33	−0.68	0.45
	Ligustrum lucidum	SR	5.63	40.85	0.37	2.67	0.27
		ER	6.12	42.36	−0.33	−2.36	0.33
		MSR	4.72	35.80	−0.30	−2.17	0.36
	Sapindus saponaria	SR	10.73	43.32	0.54	2.18	0.35
		ER	10.35	40.75	0.23	0.93	0.41
		MSR	9.08	35.25	0.55	1.63	0.39
	Metasequoia glyptostroboides	SR	10.63	39.7	−0.58	−2.18	0.31
		ER	10.42	38.95	0.22	0.81	0.40
		MSR	7.66	30.54	0.38	1.41	0.43
	Taxodium distichum var. imbricatum	SR	10.03	40.49	−0.44	−1.97	0.26
		ER	9.42	42.53	0.35	1.58	0.37
		MSR	7.06	27.94	−0.17	−0.78	0.42

3.4. Spatial Distribution of Forest Carbon Density

3.4.1. Spatial Distribution of All-Forest Carbon Density

The spatial distribution of all forest carbon densities on Chongming eco-island (early 2020) is shown in Figure 3. The carbon density values were in the range of 1.5–72 t/ha, and the average values were 18.6 t/ha, 19.9 t/ha, 10.2 t/ha, and 13.3 t/ha for Chongming eco-island (three islands), Chongming Island, Changxing Island, and Hengsha Island, respectively (Table 4). Higher values were observed in the midwestern region of Chongming Island, where urban towns (e.g., Miao Town and Gangxi Town) and a large forest park (i.e., Dongping National Forest Park) are located. The values of urban towns were in the range of 25–45 t/ha, and the highest values were generally detected in forest parks (>50 t/ha). The carbon-density values of Changxing Island and Hengsha Island were generally lower than 15 t/ha. Regarding Chongming Island, higher carbon density values were generally observed in the southern and western regions, opposite to what was observed in the eastern and northern regions. The total forest carbon storage of the three Chongming islands was 573,123.6 t, among which the total carbon storage proportions were 90.32% for Chongming Island, 4.86% for Changxing Island, and 4.82% for Hengsha Island (Table 4).

Table 3. Accuracy value comparisons of carbon density among machine learning models and different forest classification schemes. EBLF: evergreen broad-leaved forest, DBLF: deciduous broad-leaved forest, WCF: warm coniferous forest; RF: random forest model, DT: decision tree model, and NN: neural network model.

Classification Scale		Model Name	RMSE (t/ha)	rRMSE (%)	Bias (t/ha)	rBias (%)	R^2
Forest type	All forests	RF	6.45	25.82	−0.35	−1.40	0.59
		NN	10.77	43.08	0.43	1.72	0.48
		DT	10.43	41.72	−0.41	−1.62	0.42
	EBLF	RF	6.32	23.73	0.11	0.43	0.77
		NN	7.69	29.69	−0.19	−0.74	0.44
		DT	8.68	33.51	0.17	0.64	0.51
	DBLF	RF	6.58	23.01	0.25	0.88	0.68
		NN	10.04	35.12	0.31	0.92	0.58
		DT	5.71	19.97	0.23	0.81	0.68
	WCF	RF	5.45	20.49	−0.18	−0.68	0.67
		NN	7.97	29.96	−0.16	−0.60	0.50
		DT	5.90	22.18	0.08	0.30	0.62
Dominant tree species	*Cinnamomum camphora*	RF	7.06	18.83	−0.15	−0.39	0.75
		NN	7.62	20.32	0.16	0.41	0.43
		DT	8.83	23.55	0.24	0.63	0.71
	Ligustrum lucidum	RF	3.96	28.91	0.12	0.85	0.64
		NN	3.15	23.48	−0.16	−1.16	0.52
		DT	2.62	19.12	0.07	0.46	0.65
	Sapindus saponaria	RF	7.83	31.58	−0.13	−0.54	0.68
		NN	4.43	30.77	0.24	0.95	0.37
		DT	5.52	22.27	0.20	0.51	0.71
	Metasequoia glyptostroboides	RF	6.95	25.12	0.18	0.67	0.66
		NN	5.63	20.97	−0.22	−0.81	0.53
		DT	4.86	17.98	−0.06	−0.23	0.73
	Taxodium distichum var. imbricatum	RF	6.91	30.63	0.14	0.62	0.60
		NN	7.72	33.21	−0.26	−1.17	0.41
		DT	5.78	25.79	0.10	0.43	0.63

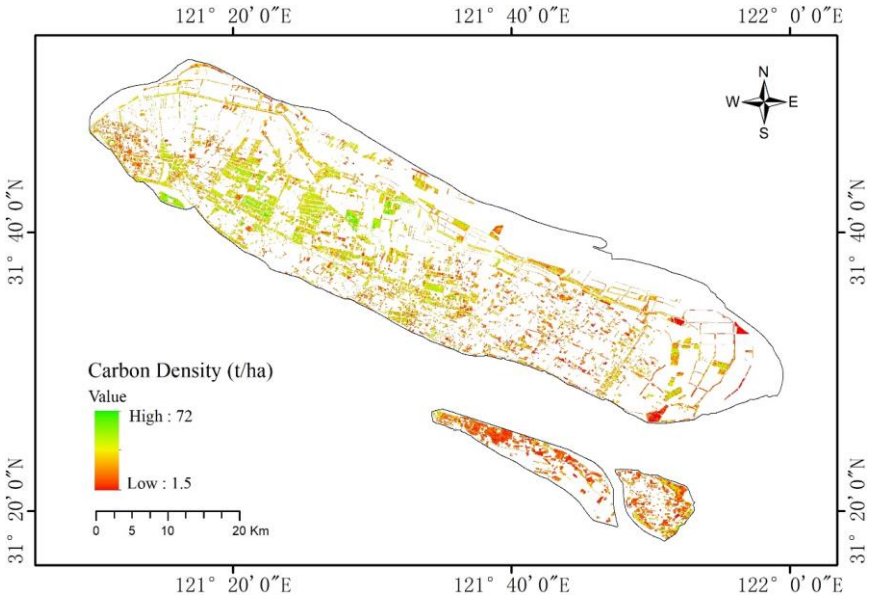

Figure 3. Spatial distribution of the forest carbon density at the all-forest classification scale on Chongming eco-island.

3.4.2. Spatial Distribution of Forest Carbon Density by Forest Type

The spatial distribution of the forest carbon density by forest type in Chongming eco-island is shown in Figure 4. For each forest type, large carbon density value differences were observed in the spatial distribution, mainly ranging from 2–65 t/ha. For evergreen broad-leaved forests, the total carbon storage amount and average carbon density value

were 305,403.3 t and 19.2 t/ha, respectively (Table 4). The higher carbon density values were distributed in mid-western regions, opposite to what was observed on Changxing Island and Hengsha Island (Figure 4a). Regarding deciduous broad-leaved forests, the total carbon storage amount and average carbon density value were 187,769.4 t and 18.1 t/ha, respectively (Table 4). This forest type was distributed mainly on Chongming Island, and higher values were distributed in the western and eastern regions of Chongming Island (Figure 4b). For warm coniferous forests, the total carbon storage amount and average carbon density value were 79,950.9 t and 17.2 t/ha (Table 4), respectively, and higher values were generally observed in forest parks (e.g., Dongping forest park) and landscape forests along coastal dams and rivers, opposite to what was observed in the eastern part of Chongming Island (Figure 4c). The contributions of forest carbon storage from each forest type (evergreen broad-leaved forests, deciduous broad-leaved forests, and warm coniferous forests) to the total amount were 53.29%, 32.76%, and 13.95%, respectively (Table 4).

Table 4. Average forest carbon density (t/ha) and carbon storage across Chongming eco-island (three islands) at the scales of different forest types and dominant tree species. EBLF: evergreen broad-leaved forest, DBLF: deciduous broad-leaved forest, and WCF: warm coniferous forest.

		Carbon Density (t/ha)	Carbon Storage (t)	Percentage (%)
Area	Chongming island	19.9	517,660.6	90.32
	Changxing island	10.2	27,825.6	4.86
	Hengsha island	13.3	27,637.4	4.82
	Chongming three islands	18.6	573,123.6	100
Forest type	EBLF	19.2	305,403.3	53.29
	DBLF	18.1	187,769.4	32.76
	WCF	17.2	79,950.9	13.95
Dominant tree species	*C. camphora*	23.7	221,832.5	38.71
	L. lucidum	14.6	50,370.2	8.79
	T. distichum var. imbricatum	17.7	26,904.4	4.69
	M. glyptostroboide	19.8	46,728.8	8.15
	S. saponaria	20.5	45,715.0	7.98
	Total amount		391,550.9	68.32

Note: Percentages (%) indicates the proportion of carbon storage of each island, forest types, or tree species to the total carbon storage.

3.4.3. Spatial Distribution of Forest Carbon Density by Dominant Tree Species

The spatial distribution of the forest carbon density by dominant tree species on Chongming eco-island is shown in Figure 5. For *C. camphora*, the forest carbon density values were in the range of 12–55 t/ha, the average carbon density value was 23.7 t/ha with a relatively even distribution, and the carbon storage was 221,832.5 t, accounting for 38.71% of the total forest carbon storage (Figure 5a; Table 4). Regarding *L. lucidum*, the forest carbon density values were in the range of 3–25 t/ha, with higher values distributed mainly in the midwestern region of Chongming Island. The average carbon density value was 14.6 t/ha, and the carbon storage value was 50,370.2 t, accounting for 8.79% of the total forest carbon storage (Figure 5b; Table 4). For *T. distichum var. imbricatum*, the forest carbon density values were in the range of 5–55 t/ha, the average carbon density value was 17.7 t/ha, and the carbon storage amount was 26,904.4 t, accounting for 4.69% of the total forest carbon storage (Figure 5c; Table 4). For *M. glyptostroboides*, the forest carbon density values were in the range of 5–70 t/ha, and the highest values could be observed in forest parks. The average carbon density value was 19.8 t/ha, and the carbon storage amount was 46,728.8 t, accounting for 8.15% of the total forest carbon storage (Figure 5d; Table 4). For *S. saponaria*, the forest carbon density values were in the range of 5–50 t/ha, with higher values distributed mainly in the midwestern region of Chongming Island. The average carbon density value was 20.5 t/ha, and the carbon storage amount was 45,715.0 t, accounting for 7.98% of the total forest carbon storage (Figure 5e; Table 4).

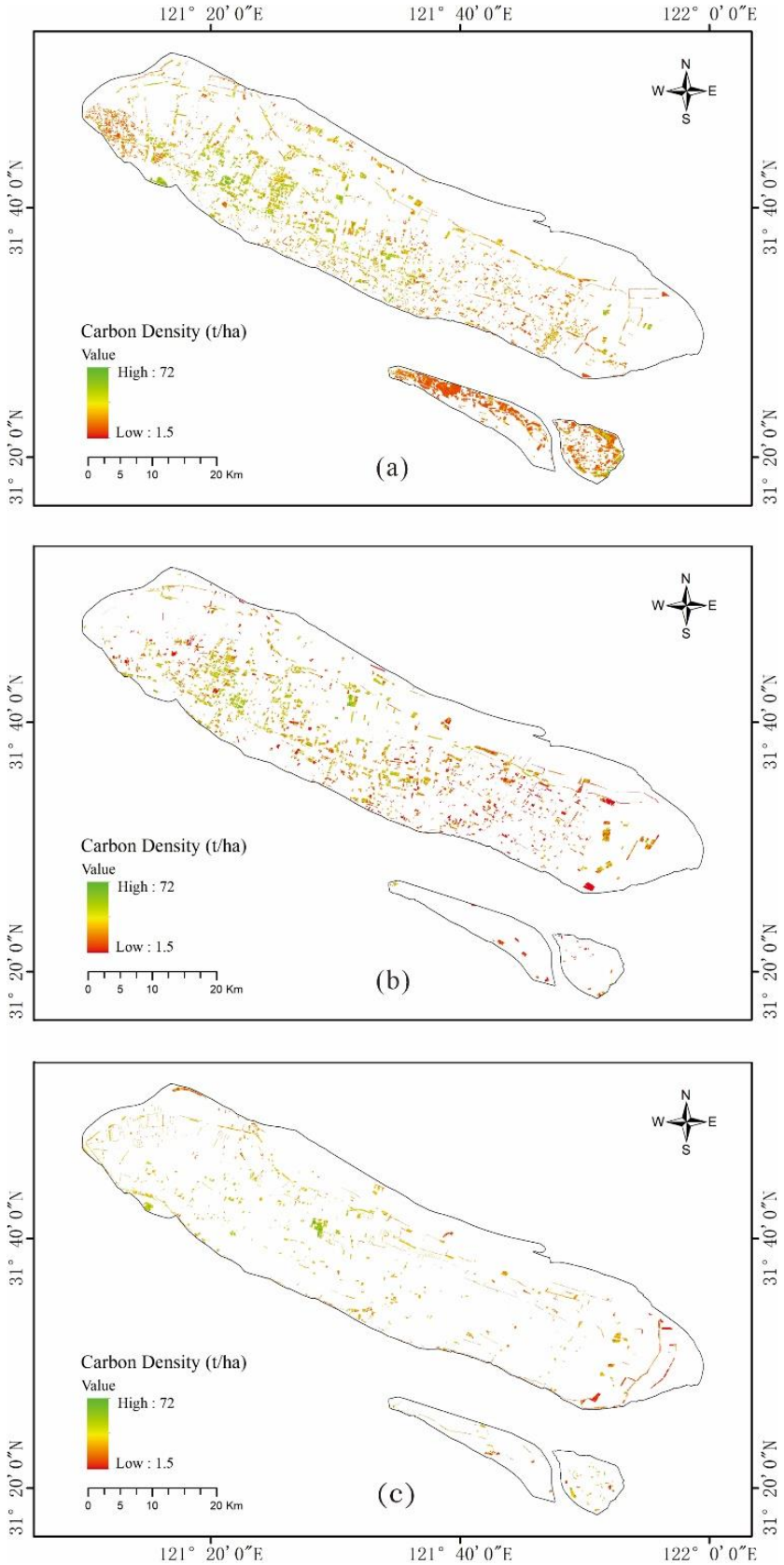

Figure 4. Spatial distribution of the forest carbon density on Chongming eco-island: (**a**) evergreen broad-leaved forests, (**b**) deciduous broad-leaved forests, and (**c**) warm coniferous forests.

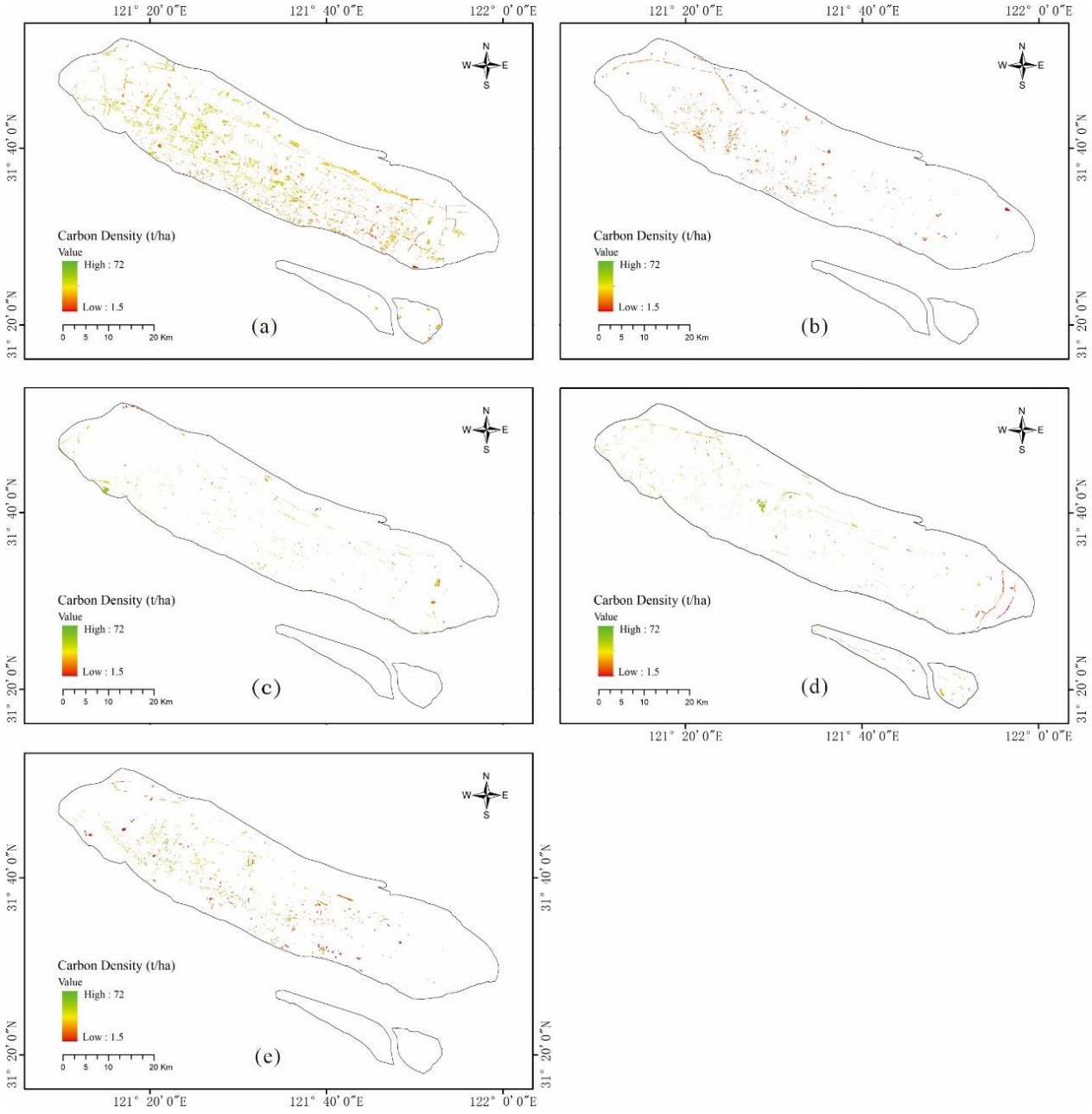

Figure 5. Spatial distribution of the forest carbon density by dominant tree species on Chongming eco-island: (**a**) *C. camphora*, (**b**) *L. lucidum*, (**c**) *T. distichum* var. *imirricatum*, (**d**) *M. glyptostroboides*, and (**e**) *S. saponaria*.

4. Discussion

4.1. Forest Carbon Storage Estimation Model Optimization

Our results showed that the machine learning models exhibited lower rRMSE and rBias values than the simple regression models across the three analyzed classification scales (Tables 2 and 3), indicating that the machine learning models had performed best in estimating forest carbon density in this study; this finding is consistent with the results of Wu et al., (2016) and Günlü et al., (2020) [40,41]. The reason for this result involves the complex nonlinear relationships between forest carbon density and optical remote sensing signals. Machine learning models, as data-driven nonparametric estimation methods, can construct high-precision estimation models between features and outputs from a large amount of training sample data compared to traditional linear regression models [42].

To date, studies regarding remote sensing-based estimations of forest carbon density by forest type are still limited [18]. In this study, estimations across three classification scales (i.e., the all-forest, forest-type, and tree-species scales) were conducted, and we found that estimation accuracies were generally higher at the forest scale than at the all-forest scale, which was in agreement with the results of Li et al., (2020) [18], this is the effect from stratified sampling, as all the pixels were relatively uniform within each stratum; consequently, the within-stratum prediction accuracy of the respective models was generally higher. On the other hand, the tree-species-scale forest carbon density estimations conducted in urban areas had not been reported previously. We found that the carbon density estimation accuracy at the tree-species scale was not significantly improved compared to the accuracy obtained at the forest-type scale (Tables 2 and 3). The reason for this result was that the forest on Chongming eco-island came mainly from human plantations, so the number of tree species corresponding to each forest type was limited; for example, the distribution area of *C. camphor* accounted for approximately 62% of the total area of evergreen tree species, and the morphologies (i.e., the heights and canopy structures) of three warm coniferous tree species (i.e., *M. glyptostroboides*, *T. distichum* var. *imbricatum*, and *Cryptomeria japonica var. sinensis Miquel*) were very similar.

The coefficients of the model represent the relationship between remotely sensed images (May 2020) and measured field data (March–August 2021), and since they can be adjusted based on field data, the one-year gap between the images and ground measurements should not affect the estimation accuracy [43]. However, it is still unclear whether oversaturation of relevant vegetation indices might occur due to differences in forest canopy structure and coverage among different forest types or tree species, which could increase uncertainty in model estimation and require further research. This study was also limited by the fact that texture information was not considered in the model optimization, and 308 sample plots (20 m × 20 m) were surveyed, which required significant labor and time. Therefore, methods to ensure or improve estimation accuracy with smaller sample sizes should be explored, which would be more practical for real-world operations.

4.2. Comparison of the Forest Carbon Density with Other Urban Cities

The forest carbon density values of Chinese urban cities were in the range of 10.2–25.6 t/ha, and the forest carbon density value of Chongming eco-island (18.6 t/ha) was also in this range and was very close to the carbon density value (18.9 t/ha) of Chongming eco-island reported by Shen et al., (2020) [11]; however, these values were lower than that of Shanghai city center (21.2 t/ha) [11] (Table 5). The reasons for this finding were as follows: (1) Chongming eco-island underwent extensive afforestation between 2006 and 2019, during which time the forest coverage nearly doubled from 15.9% to 27.4% (mainly on Chongming Island), resulting in a large distribution proportion of young forests currently compared to those in the Shanghai urban area and other urban areas, and (2) relatively low forest carbon density values were distributed on Changxing Island and Hengsha Island. More specifically, Changxing Island was positioned as a marine equipment island (land for the shipping industry), and a large area of orange plants was preserved in its western region. Additionally, Hengsha Island is still preserved now, and agriculture is still the main land use type on this island, so the forest carbon densities were relatively low on these two islands (Table 4).

Table 5. Comparison of the urban forest carbon density (t/ha) among cities in China.

Urban Region	Carbon Density (t/ha)	Reference
Chongming eco-island (three islands)	18.6	This study
Chongming island	19.9	
Changxing island	10.2	
Hengsha island	13.3	
Chongming three islands	18.9	[11]
Shanghai District	21.2	[11]

Table 5. *Cont.*

Urban Region	Carbon Density (t/ha)	Reference
Hangzhou	16.5	[44]
Ganzhou	25.6	[45]
Xi'an	20.8	[46]
Chengdu	19.9	[47]
Guangzhou	24.7	[48]
Shenzhen	24.6	[49]
Nanjing	16.9	[50]
Xiamen	15.1	[51]

4.3. Management Suggestions for Forest Carbon Storage Enhancement

The total forest coverage of Chongming eco-island was approximately 27.0% in early 2020, implying that forest plantation should be continued in the context of the carbon neutrality target and the construction of a world-class ecological island. The forest carbon density did not differ significantly among the three forest types (17.2–19.2 t/ha) (Table 4), probably because these different forest types are mainly in their early or middle growing stages, whereas the carbon density varied greatly among tree species (14.6–23.7 t/ha) (Table 4). Therefore, the selection of tree species with relatively high potential carbon storage should be considered for further plantation rather than the forest type under present planting densities. Given the current low forest carbon densities on Chongming's three islands (Table 3), and that carbon uptake is usually higher in young forests than in mature forests [52], the scientific forest management (e.g., water, nutrients, and pest control) of these forests is necessary. Additionally, trees were planted mainly from seedlings or as small trees at very high densities (i.e., 2500–10,000 trees/ha) following the standards of the local technical regulations [53], and forest thinning has not been carried out to date alongside tree growth, so optimized forest-thinning strategies aiming to improve the ecosystem carbon sink capacity should be studied and initiated in the future.

5. Conclusions

In early 2020, Chongming eco-island had a total forest area of 307.8 km^2 and carbon storage of 573,123.6 t. The forests on Chongming eco-island had relatively low carbon densities (18.6 t/ha) compared to the central district of Shanghai. The total forest carbon storage was dominated by evergreen broad-leaved forests and five dominant tree species. At refined forest classification scales, machine learning models had a combined effect that improved the carbon density estimation accuracies of urban forests. Specifically, the average rRMSE and rBias values decreased by 45.30% and 72.03%, respectively, and R^2 increased by 87.50% compared to simple regression models at the all-forests classification scale.

Supplementary Materials: The following supporting information can be downloaded at: https://www.mdpi.com/article/10.3390/rs15061575/s1, Figure S1: Number of sampling plots surveyed during March–August 2021; Table S1: Acquisition date and cloud coverage (%) of the images from Sentinel-2A used in this study; Table S2: Nineteen spectral indices used in this study; Table S3: Carbon content coefficients of the main tree species considered in this study; Table S4: Allometric biomass equations of each tree species considered in this study; Table S5: Correlation coefficients between the forest carbon densities and the spectral indices at three classification scales; Table S6: Summary of predictive variables for carbon density estimation of simple regression models and across three classification scales; Table S7: Summary of predictive variables for carbon density estimation of three machine learning models and across three classification scales. References [35,36,54–70] are cited in the Supplementary Materials.

Author Contributions: Conceptualization, C.Z. and R.S.; methodology, C.Z., T.S. and N.W.; software, T.S.; validation, W.Z.; formal analysis, Z.H. and N.W.; investigation, T.S., N.W., H.Z. and W.Z.; data curation, T.S. and H.Z.; writing—original draft preparation, C.Z. and T.S.; writing—review and editing, Z.H. and R.S.; visualization, H.Z.; supervision, R.S.; project administration, C.Z.; funding acquisition, C.Z. and R.S. All authors have read and agreed to the published version of the manuscript.

Funding: This work was funded by the Shanghai Municipal Natural Science Foundation (No 22ZR1421500), the National Natural Science Foundation of China (U2243207), the Fundamental Research Funds for Central Universities (East China Normal University), and the International Cooperation Platform of Resources, Environment and Ecology, East China Normal University.

Data Availability Statement: The Sentinel-2A data comes from European Space Agency (https://scihub.copernicus.eu/dhus/#/home (accessed on 3 May 2020)).

Acknowledgments: Great thanks are given to the students from the School of Geographic Sciences, East China Normal University, for their help with the fieldwork.

Conflicts of Interest: The authors declare no conflict of interest.

References

1. Ribeiro, H.V.; Rybski, D.; Kropp, J.P. Effects of changing population or density on urban carbon dioxide emissions. *Nat. Commun.* **2019**, *10*, 3204. [CrossRef]
2. Song, Y.C. Several issues in urban forest research. *J. Chin. Urban For.* **2004**, *1*, 4–9.
3. Lee, S.; Yim, J.; Son, Y.; Son, Y.; Kim, R. Estimation of Forest Carbon Stocks for National Greenhouse Gas Inventory Reporting in South Korea. *Forests* **2018**, *9*, 625. [CrossRef]
4. Węgiel, A.; Polowy, K. Aboveground Carbon Content and Storage in Mature Scots Pine Stands of Different Densities. *Forests* **2020**, *11*, 240. [CrossRef]
5. Strohbach, M.W.; Haase, D. Above-ground carbon storage by urban trees in Leipzig, Germany: Analysis of patterns in a European city. *Landsc. Urban Plan.* **2012**, *104*, 95–104. [CrossRef]
6. Sun, Y.; Xie, S.; Zhao, S. Valuing urban green spaces in mitigating climate change: A city-wide estimate of aboveground carbon stored in urban green spaces of China's Capital. *Glob. Chang. Biol.* **2019**, *25*, 1717–1732. [CrossRef]
7. Godwin, C.; Chen, G.; Singh, K.K. The impact of urban residential development patterns on forest carbon density: An integration of LiDAR, aerial photography and field mensuration. *Landsc. Urban Plan* **2015**, *136*, 97–109. [CrossRef]
8. Xiao, J.; Chevallier, F.; Gomez, C.; Guanter, L.; Hicke, J.A.; Huete, A.R.; Ichii, K.; Ni, W.; Pang, Y.; Rahman, A.F.; et al. Remote sensing of the terrestrial carbon cycle: A review of advances over 50 years. *Remote Sens. Environ.* **2019**, *233*, 111383. [CrossRef]
9. Ren, Z.; Zheng, H.; He, X.; Zhang, D.; Yu, X.; Shen, G. Spatial estimation of urban forest structures with Landsat TM data and field measurements. *Urban For. Urban Green.* **2015**, *14*, 336–344. [CrossRef]
10. Sun, H.; Qie, G.; Wang, G.; Tan, Y.; Li, J.; Peng, Y.; Ma, Z.; Luo, C. Increasing the Accuracy of Mapping Urban Forest Carbon Density by Combining Spatial Modeling and Spectral Unmixing Analysis. *Remote Sens.* **2015**, *7*, 15114–15139. [CrossRef]
11. Shen, G.; Wang, Z.; Liu, C.; Han, Y. Mapping aboveground biomass and carbon in Shanghai's urban forest using Landsat ETM+ and inventory data. *Urban For. Urban Green.* **2020**, *51*, 126655. [CrossRef]
12. Myeong, S.; Nowak, D.J.; Duggin, M.J. A temporal analysis of urban forest carbon storage using remote sensing. *Remote Sens. Environ.* **2006**, *101*, 277–282. [CrossRef]
13. Amoatey, P.; Sulaiman, H.; Kwarteng, A.; Al-Reasi, H.A. Above-ground carbon dynamics in different arid urban green spaces. *Environ. Earth Sci.* **2018**, *77*, 431. [CrossRef]
14. Uniyal, S.; Purohit, S.; Chaurasia, K.; Rao, S.S.; Amminedu, E. Quantification of carbon sequestration by urban forest using Landsat 8 OLI and machine learning algorithms in Jodhpur, India. *Urban For. Urban Green.* **2022**, *67*, 127445. [CrossRef]
15. Mngadi, M.; Odindi, J.; Mutanga, O. The Utility of Sentinel-2 Spectral Data in Quantifying Above-Ground Carbon Stock in an Urban Reforested Landscape. *Remote Sens.* **2021**, *13*, 4281. [CrossRef]
16. Zhang, F.; Tian, X.; Zhang, H.; Jiang, M. Estimation of aboveground carbon density of forests using deep learning and multisource remote sensing. *Remote Sens.* **2022**, *14*, 3022. [CrossRef]
17. Ahmad, A.; Gilani, H.; Ahmad, S.R. Forest Aboveground Biomass Estimation and Mapping through High-Resolution Optical Satellite Imagery—A Literature Review. *Forests* **2021**, *12*, 914. [CrossRef]
18. Li, L.; Zhou, X.S.; Chen, L.Q.; Chen, L.G.; Zhang, Y.; Liu, Y.Q. Estimating urban vegetation biomass from Sentinel-2A image data. *Forests* **2020**, *11*, 125. [CrossRef]
19. Shanghai Municipal Government. *Shanghai Carbon Peaking Action Plan*; Shanghai Municipal Government: Shanghai, China, 2022.
20. Dong, H.; Qian, L.; Yan, J.; Wang, L. Evaluation of the carbon accumulation capability and carbon storage of different types of wetlands in the Nanhui tidal flat of the Yangtze River estuary. *Environ. Monit. Assess.* **2020**, *192*, 585. [CrossRef]
21. Qian, L.W.; Yan, J.F.; Hu, Y.; Gao, L.Y.; Wu, P.F.; Wang, L. Spatial distribution patterns of annual soil carbon accumulation and carbon storage in the Jiuduansha wetland of the Yangtze River estuary. *Environ. Monit. Assess.* **2019**, *191*, 750. [CrossRef]

22. Wang, R.J.; Zhao, M.; Gao, J. Carbon storage of main vegetation types of urban forest, Chongming Island of China. *Sci. Geog. Sin.* **2011**, *31*, 490–494.
23. Zhong, Q.C.; Fu, Y.; Zhang, G.L. Biomass estimation and a dynamic analysis of forests in Shanghai. *J. Zhejiang Agric. For. Univ.* **2019**, *36*, 524–532.
24. Zhang, G.L. Spatial distribution characteristics of carbon storage of urban forests in Shanghai based on remote sensing estimation. *Ecol. Env. Sci.* **2021**, *30*, 1777–1786.
25. Kokubu, Y.; Hara, S.; Tani, A. Mapping seasonal tree canopy cover and leaf area using Worldview-2/3 Satellite Imagery: A megacity-scale case study in Tokyo urban area. *Remote Sens.* **2020**, *12*, 1505. [CrossRef]
26. Shanghai Municipal Government. *Overall Plan for Chongming Three Islands*; Shanghai Municipal Government: Shanghai, China, 2006.
27. Shanghai Municipal Government. *Chongming District Master Plan & Land Utilization Master Plan (2017–2035)*; Shanghai Municipal Government: Shanghai, China, 2018.
28. Xie, L.J.; Flynn, A.; Tan-Mullins, M.; Cheshmehzangi, A. Water and land: Environmental governance and Chinese eco-development. *J. Clean. Prod.* **2019**, *221*, 839–853. [CrossRef]
29. Chang, M.Y. Diversity and Vegetation Characteristics of Vascular Plants in Chongming, Shanghai. Master's Thesis, East China Normal University, Shanghai, China, 2022.
30. Zhang, Z.S. Study on the Characteristics of Plantation Community and Soil Physicochemical Properties in Chongming Island. Master's Thesis, East China Normal University, Shanghai, China, 2010.
31. Editorial Committee for Vegetation of China. *Vegetation of China*; Science Press: Beijing, China, 1980.
32. Meng, C.; Li, Q.; Yang, M.; Tang, Y.J. Study on individual tree recognition technology of high resolution aerial remote sensing image based on Deep Learning. *Mod. Surv. Mapp.* 2023; *accepted*.
33. Da, L.J.; Yang, T.H.; Song, Y.C. Study on the urban ecological regionalization and forest distribution in Shanghai, China. *Sci. Silvae. Sin.* **2004**, *40*, 84–88.
34. Sun, W. The Type, Distribution and Coordination Evaluation of the Main Plant Communities in Chongming Island and Their Ecological Landscape. Master's Thesis, East China Normal University, Shanghai, China, 2013.
35. Dang, A.T.N.; Nandy, S.; Srinet, R.; Luong, N.V.; Ghosh, S.; Kumar, A.S. Forest aboveground biomass estimation using machine learning regression algorithm in Yok Don National Park, Vietnam. *Ecol. Inform.* **2019**, *50*, 24–32. [CrossRef]
36. Sims, D.A.; Gamon, J.A. Relationships between leaf pigment content and spectral reflectance across a wide range of species, leaf structures and developmental stages. *Remote Sens. Environ.* **2002**, *81*, 337–354. [CrossRef]
37. Nandy, S.; Srinet, R.; Padalia, H. Mapping forest height and aboveground biomass by integrating ICESat-2, Sentinel-1 and Sentinel-2 data using Random forest algorithm in northwest Himalayan foothills of India. *Geophys. Res. Lett.* **2021**, *48*, e2021GL093799. [CrossRef]
38. Chen, L.; Ren, C.Y.; Zhang, B.; Wang, Z.M.; Xi, Y.B. Estimation of Forest Above-Ground Biomass by Geographically Weighted Regression and Machine Learning with Sentinel Imagery. *Forests* **2018**, *9*, 582. [CrossRef]
39. Liu, C.; Li, X. Carbon storage and sequestration by urban forests in Shenyang, China. *Urban For. Urban Green.* **2012**, *11*, 121–128. [CrossRef]
40. Wu, C.; Shen, H.; Shen, A.; Deng, J.; Gan, M.; Zhu, J.; Xu, H.; Wang, K. Comparison of machine-learning methods for above-ground biomass estimation based on Landsat imagery. *J. Appl. Remote Sens.* **2016**, *10*, 35010. [CrossRef]
41. Günlü, A.; Keleş, S.; Ercanli, İ.; Şenyurt, M. *Estimation of Aboveground Stand Carbon Using Landsat 8 OLI Satellite Image: A Case Study from Turkey*; Springer International Publishing: Cham, Switzerland, 2020; pp. 385–403.
42. Markus, R.; Gustau, C.; Bjorn, S.; Martin, J.; Joachim, D.; Nuno, C. Deep learning and process understanding for data-driven earth system science. *Science* **2019**, *566*, 195–204.
43. Hou, Z.; Xu, Q.; McRoberts, R.E.; Greenberg, J.A.; Liu, J.; Heiskanen, J.; Pitkänen, S.; Packalen, P. Effects of temporally external auxiliary data on model-based inference. *Remote Sens. Environ.* **2017**, *198*, 150–159. [CrossRef]
44. Zhang, J.C. Biomass Estimation of Urban Lands and Analysis of Its Spatio-Temporal Variation in Hangzhou City. Master's Thesis, Zhejiang A&F University, Hangzhou, China, 2014.
45. Zeng, G.L. Research on the Change of Vegetation Coverage and Carbon Storage Based on Remote Sensing-Take Ganzhou City as an Example. Master's Thesis, Jiangxi University of Science and Technology, Nanchang, China, 2017.
46. Zhang, H. Vegetation Carbon Storage in Xi'an in Recent Years Dynamic Responses to Land-Use Cover Change. Master's Thesis, Shaanxi Normal University, Xi'an, China, 2011.
47. Ren, D.Z.; Liao, X.Y.; Xiao, Q.G.; Lai, C.H.; Song, F.; Meng, S.M. Carbon storage and spatial distribution pattern of forest vegetation in Chengdu. *J. West China For. Sci.* **2021**, *50*, 74–81.
48. Kang, W.X.; Tian, Z.; He, J.N.; Cui, S.S. Carbon cycle in ten kinds of forest ecosystem in Guangzhou City. *Chin. J. Appl. Ecol.* **2009**, *20*, 2917–2924.
49. Ye, J.S.; She, G.H. Forest carbon dynamics in Guangdong province. *J. Nanjing For. Univ.* **2010**, *34*, 7–12.
50. Wang, Z.H.; Liu, H.M.; Guan, Q.W.; Wang, X.J.; Hao, J.P.; Ling, N.; Shi, C. Carbon storage and density of urban forest ecosystems in Nanjing. *J. Nanjing Forestry Univ.* **2011**, *35*, 18–22.
51. Ren, Y.; Wei, X.; Wei, X.; Pan, J.; Xie, P.; Song, X.; Peng, D.; Zhao, J. Relationship between vegetation carbon storage and ur-banization: A case study of Xiamen, China. *For. Ecol. Manag.* **2011**, *261*, 1214–1223. [CrossRef]

52. Houghton, R.A. Above ground forest biomass and the global carbon balance. *Glob. Chang. Biol.* **2005**, *11*, 945–958. [CrossRef]
53. Shanghai Municipal Bureau of Agriculture and Forestry. *Technical Regulations for the Construction of Ecological Public Welfare Forests in Shanghai*; Shanghai Municipal Bureau of Agriculture and Forestry: Shanghai, China, 2003.
54. Zhang, H.A. Measurement and analysis of carbon content rates of eight tree species in Guangdong Province. *For. Resour. Manag.* **2018**, *1*, 148–154.
55. Xu, Q.H.; Lin, L.P.; Xue, C.Q.; Luo, Y.; Lei, Y.C. Component specific carbon content and storage of *Cinnamomum camphora* in Guangdong Province. *J. Zhejiang Agri. For. Univ.* **2019**, *36*, 70–79.
56. Ma, J.Q.; Li, G.Y.; Tian, L. Comparative study on carbon rate of main afforestation tree species in Henan Province. *J. Henan Agri. Sci.* **2012**, *41*, 131–132.
57. Bai, B.X.; Jiao, S.D.; Chen, D.H. The biomass and carbon fixation of 38 tree species in northern and central region of Henan Province. *J. West China For. Sci.* **2017**, *46*, 79–84.
58. Fan, X.; Tian, D.L.; Fan, W.; Yang, H.Q. Carbon content of main agro-forestry tree species in the North China Plain. *J. Cent. South Univ. For. Technol.* **2014**, *34*, 85–93.
59. Tang, X.; Huang, C.D.; Zhang, J.; Ning, Y.C. An Analysis of the carbon content rate in main coniferous species in Sichuan. *J. Sichuan For. Sci. Technol.* **2007**, *02*, 20–23.
60. Tian, Y.Y. Research on Forest Carbon Stocks Based on Forest Resources Census in Xuzhou. Master's Thesis, Nanjing Forestry University, Nanjing, China, 2012.
61. Wang, L. Study on the Carbon Sequestration Capabilities of Common Tree Species and Communities in Main District of Chongqing City. Master's Thesis, Southwest University, Chongqing, China, 2013.
62. Tian, Y.Y.; Qin, F.; Yan, H.; Guo, W.H.; Guan, Q.W. Carbon content rate in the common woody plants of China. *J. Anhui Agric. Sci.* **2011**, *39*, 16166–16169.
63. Zhang, T. Study on the Carbon Stock of Planation in the Xuyi. Master's Thesis, Nanjing Forestry University, Nanjing, China, 2015.
64. Zhu, M. Study on the Carbon Fixation Evaluate of the Green-Land System in the Xi'an ChanBa Eco-Region. Master's Thesis, Xi'an University of Architecture and Technology, Xi'an, China, 2020.
65. Zhu, Y.Y. Characteristics of Structure and Carbon Storage of Greening on the Campus of Anhui Agricultural University. Master's Thesis, Anhui Agricultural University, Hefei, China, 2016.
66. Sun, Q.X.; Yu, F.A.; Peng, Z.H. Study on poplar plantation biomass in Yangtze River beach. *For. Sci. Technol.* **1998**, *3*, 3–5.
67. He, H.Z.; Huang, L.H.; Duan, X.; He, R.K. Study on biomass in main afforestation tree species of the second ring forest-belt of Guiyang. *Guizhou Sci.* **2007**, *3*, 33–39.
68. Wang, Z.; Han, Y.J.; Kang, H.Z.; Huang, D.; Xue, C.Y.; Yin, S.; Liu, C.J. Carbon storage of main tree species plantations for water resources conservation in upper reaches of Huangpu River, Shanghai. *Chinese J. Ecol.* **2012**, *31*, 1930–1935.
69. Zhang, X.J.; Leng, H.B.; Zhao, G.Q.; Jing, J.; Tu, A.C.; Song, K.; Da, L.J. Allometric models for estimating aboveground biomass for four common greening tree species in Shanghai City, China. *J. Nanjing For. Univ.* **2018**, *42*, 141–146.
70. Lin, Q.S.; Hong, W.; Wu, C.Z.; Lin, Y.M.; Chen, C. Organic carbon storage and its dynamic change in citrus ecosystem in Yongchun, China. *Acta Ecol. Sin.* **2010**, *30*, 309–316.